Evolution of Enzymatic Activities in the Orotidine 5′-Monophosphate Decarboxylase Suprafamily: Structural Basis for Catalytic Promiscuity in Wild-Type and Designed Mutants of 3-Keto-L-gulonate 6-Phosphate Decarboxylase†

Eric L. Wise,‡ Wen Shan Yew,§ Julie Akana,§ John A. Gerlt,*,§ and Ivan Rayment*,‡

Department of Biochemistry, University of Wisconsin, Madison, Wisconsin 53706, and Departments of Biochemistry and Chemistry, University of Illinois, Urbana, Illinois 61801

Received October 12, 2004; Revised Manuscript Received November 16, 2004

ABSTRACT: 3-Keto-L-gulonate 6-phosphate decarboxylase (KGPDC) and D-*arabino*-hex-3-ulose 6-phosphate synthase (HPS), members of the orotidine 5′-monophosphate decarboxylase (OMPDC) suprafamily, catalyze reactions that involve the formation of Mg^{2+}-ion stabilized 1,2-enediolate intermediates. The active sites of KGPDC and HPS share several conserved residues, including the presumed ligands for the Mg^{2+} and a catalytic histidine residue that has been implicated in protonation of the intermediate in the KGPDC-catalyzed reaction. As reported in the previous manuscript, both enzymes are naturally promiscuous, with KGPDC from *Escherichia coli* catalyzing a low level of the HPS reaction and the HPS from *Methylomonas aminofaciens* catalyzing a significant level of the KGPDC reaction. Interestingly, the promiscuous HPS reaction catalyzed by KGPDC can be significantly enhanced by replacing no more than four active site residues from KGPDC reaction with residues from HPS. In this manuscript, we report structural studies of wild-type and mutant KDGPC's that provide a structural explanation for both the natural promiscuity for the HPS reaction and the enhanced HPS activity and diminished KGPDC activity catalyzed by active site mutants.

3-Keto-L-gulonate 6-phosphate decarboxylase (KGPDC)[1] and D-*arabino*-hex-3-ulose 6-phosphate synthase (HPS) are members of the orotidine 5′-monophosphate decarboxylase (OMPDC) suprafamily (*1*). KGPDC catalyzes the formation of L-xylulose 5-phosphate and carbon dioxide from 3-keto-L-gulonate 6-phosphate in the anaerobic pathway for L-ascorbate utilization in some eubacteria; HPS catalyzes the formation of D-*arabino*-hex-3-ulose 6-phosphate from D-ribulose 5-phosphate and formaldehyde in microorganisms that can assimilate formaldehyde as a carbon source (Scheme 1) (*2*−*8*). In contrast to the reaction catalyzed by OMPDC, both KGPDC and HPS catalyze reactions that involve the Mg^{2+}-assisted formation and stabilization of 1,2-enediolate intermediates.

Earlier structural studies established that, like OMPDC, KGPDC assembles as a dimer of $(\beta/\alpha)_8$-barrels (Figure 1) (*1*). In both enzymes, two equivalent active sites are located at the dimer interface. Although a structural explanation for the impressive catalytic proficiency has not yet been generally accepted, OMPDC evidently uses a hydrogen bonded network of active site residues to avoid the formation of a highly unstable vinyl anion intermediate (*5*, *9*, *10*). The catalytically important residues are an aspartate at the end of the first β-strand, a lysine at the end of the second β-strand, and an Asp-x-Lys-x-x-Asp motif at the end of the third β−strand, with the first aspartate and lysine from one polypeptide and the second aspartate from the adjacent subunit in each active site. The lysine apparently acts as the general acid that delivers a proton to C6 to form the product (*4*, *5*). In KGPDC, the lysine at the end of the second β-strand is replaced by a glutamate (Glu 33), and the essential Mg^{2+} is liganded by this glutamate and Asp 62 of the Asp 62-x-Lys 64-x-x-Asp 67 motif at the end of the third β-strand (*11*). A key difference between the mechanisms of KGPDC and OMPDC is the identity of the catalytic acid. Lys 64, the general acid in OMPDC, does not perform a similar function in KGPDC. Instead a His 136 and Arg 139 competitively transfer protons to a 1,2-*cis*-enediolate intermediate via intervening water molecules (*12*, *13*).

† This research was supported by Grants GM-52594 (to J.A.G. and I.R.) and GM-65155 (to J.A.G. and I.R.) from the National Institutes of Health. E.L.W. was supported by NIH Biophysics Training Grant GM08293. Use of the Argonne National Laboratory Structural Biology Center beamline at the Advanced Photon Source was supported by the U.S. Department of Energy, Office of Energy Research, under Contract No. W-31-109-ENG-38. The X-ray coordinates and structure factors for KGPDC have been deposited in the Protein Data Bank (1XBV, 1XBY, 1XBX, and 1XBZ for D-ribulose 5-phosphate, E112D/T169A•D-ribulose 5-phosphate, E112D/R139V/T169A•D-ribulose 5-phosphate, and E112D/R139V/T169A•L-xylulose 5-phosphate).

* To whom correspondence should be addressed. I.R.: Department of Biochemistry, University of Wisconsin, 433 Babcock Drive, Madison, WI 53706; phone, (608) 262-0437; fax, (608) 262-1319; e-mail, Ivan_Rayment@biochem.wisc.edu. J.A.G.: Department of Biochemistry, University of Illinois, 600 South Mathews Avenue, Urbana, IL 61801; phone, (217) 244-7414; fax, (217) 265-0385, e-mail, j-gerlt@uiuc.edu.

‡ University of Wisconsin.

§ University of Illinois.

[1] Abbreviations: APS, Advanced Photon Source at Argonne National Laboratory, Argonne, IL; HPS, D-*arabino*-hex-3-ulose 6-phosphate synthase; KGPDC, 3-keto-L-gulonate 6-phosphate decarboxylase; MePEG, methyl ether poly(ethylene glycol); OMP, orotidine 5′-monophosphate; OMPDC, orotidine 5′-monophosphate decarboxylase; D-R5P, D-ribulose 5-phosphate; RMS, root mean square; L-X5P, L-xylulose 5-phosphate.

10.1021/bi0478143 CCC: $30.25
Published on Web 01/22/2005

Scheme 1: The Reactions Catalyzed by KGPDC, HPS, and OMPDC along with Proposed Reaction Intermediates or Transition States

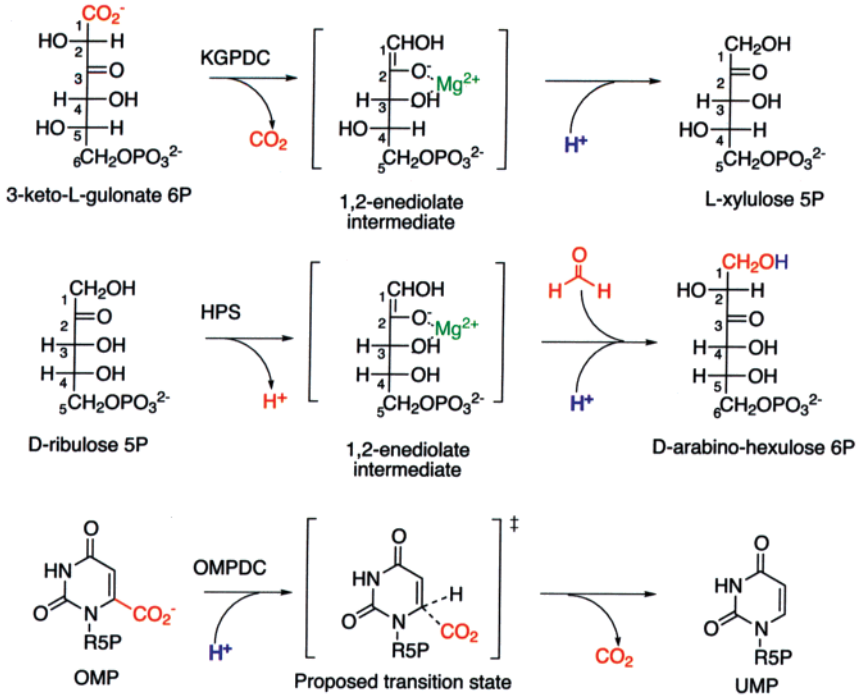

Although no structure is currently available for an HPS, it is likely that its active site will resemble that of KGPDC because of the sequence similarity between the two enzymes. In particular, the groups at the ends of the first, second, and third β-strands are conserved, thereby providing the ligands for the Mg^{2+} ion that is essential for both reactions. Although the histidine at the end of the sixth β-strand is conserved, the glutamate at the end of the fifth β-strand is replaced with an aspartate, suggesting the presence of a His-Asp dyad in HPS instead of a His-Glu dyad. No arginine is located at the end of the sixth β-strand. Because the aldol condensation is both expected to require enolization of the D-ribulose 5-phosphate substrate and reported to be stereospecific for the formation of the arabino-configured product, it is expected that the His-Asp dyad is the required general base in the HPS-catalyzed reaction. The reason for this sequence change from KGPDC is unclear.

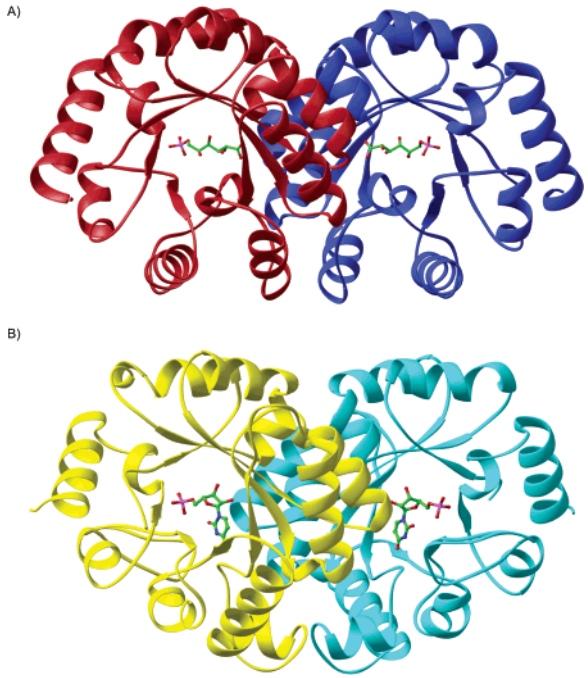

FIGURE 1: The structures of the (A) KGPDC with bound L-gulonate 6-phosphate and (B) OMPDC with bound UMP. Both enzymes adopt similar $(\beta/\alpha)_8$-barrel folds and adopt similar tertiary structures.

As reported in the previous manuscript, KGPDC catalyzes a low level of the HPS reaction and HPS catalyzes a significant level of the KGPDC reaction, thereby providing complementary functional promiscuity in the OMPDC suprafamily (*14*). Presumably, both active sites use the coordinated Mg^{2+} to stabilize 1,2-enediolate intermediates, although these are generated differently in the two enzymes: decarboxylation of 3-keto-L-gulonate 6-phosphate by KGPDC and general base-catalyzed enolization of D-ribulose 5-phosphate in HPS. The previous manuscript also reported that the promiscuous HPS reaction catalyzed by KGPDC is stereospecific and yields the same D-*arabino*-hex-3-ulose 6-phosphate product produced by the natural HPS. In contrast, the promiscuous KGPDC reaction catalyzed by HPS is stereospecific with respect to protonation of the 1,2-enediolate intermediate, with the stereochemical course consistent with the His-Asp dyad providing the proton incorporated into the L-xylulose product.

Interestingly, the promiscuous HPS activity catalyzed by KGPDC could be significantly enhanced by replacing only a few residues conserved among KGPDC's with conserved residues found in HPS's (*14*). In particular, Glu 112 at the end of the fifth β-strand was replaced with an aspartate, Arg 139 at the end of the sixth β-strand was replaced with a valine, Thr 169 at the end of the seventh β-strand was replaced with an alanine, and Arg 192 at the end of the eighth β-strand was replaced with an alanine. Although the E112D, R139V, and T196A substitutions individually enhanced the

Table 1: Data Collection Statistics

	WT·D-R5P	E112D/T169V·D-R5P	E112D/R139V/T169V·D-R5P	E112D/R139V/T169A·L-X5P
wavelength (Å)	0.900	0.961	0.961	0.961
source	APS 19-ID	APS 19-ID	APS 19-ID	APS 19-ID
unit cell dimens				
a (Å)	123.8	122.8	123.0	123.8
b, (Å)	41.5	41.9	41.8	41.5
c, (Å)	91.2	91.2	91.1	91.1
β (deg)	96.7	97.5	97.5	97.5
resolution (Å)[a]	1.70 (1.76−1.70)	1.58 (1.64−1.58)	1.80 (1.86−1.80)	1.80(1.86−1.80)
unique reflns	54902	63096	42532	42939
total reflns	382817	410568	746805	380178
completeness (%)	99.1 (98.2)	98.4 (89.8)	99.8 (100.0)	99.9 (99.6)
av I/σ[a]	15.8 (3.3)	27.7 (3.5)	17.9 (4.3)	32.3 (7.6)
R-merge[a]	0.042 (0.4377)	0.058 (0.335)	0.081 (0.240)	0.066 (0.220)

[a] The value in parentheses gives the statistics for the highest resolution shell.

promiscuous reaction ≤5-fold and the R192A substitution decreased the promiscuous reaction by ≥100-fold, multiple substitutions were synergistic, with the value of the k_{cat} for the promiscuous reaction increased 170-fold by the E112D/R139V/T169A/R192A mutant, and the value of k_{cat}/K_m increased 260-fold by the E112D/R139V/T169A mutant. For both of these multiple mutants, the values of the kinetic constants for the natural KGPDC activity were decreased.

In this manuscript, structural studies are reported that provide important insights into the observed changes in both the natural KGPDC and the promiscuous HPS reaction. The X-ray crystal structure of KGPDC with the D-ribulose 5-phosphate substrate for the HPS reaction to 2.0 Å resolution has been determined in order to understand better the nature of the catalytic promiscuity for the HPS reaction. The structures of two designed KGPDC mutants, E112D/T169A and E112D/T169A/R139V, are also described with the HPS substrate bound to 1.6 and 1.8 Å resolution, respectively. Finally, the structure of the E112D/T169A/R139V triple mutant with the L-xylulose 5-phosphate product of the KGPDC reaction has been determined. The designed substitutions were observed to have small but significant effects on the conformations of the ligands as well as in the placement of His 136 relative to the bound ligands, thereby allowing the observed changes in the values of the kinetic constants reported in the previous paper to be rationalized.

MATERIALS AND METHODS

Construction of KGPDC Mutants. Site-directed mutants of KGPDC were introduced into the *UlaD* gene, which encodes KGPDC, using the QuikChange kit (Stratagene). The DNA sequences of each mutant were verified, and the protein was expressed in the BLR(DE3) *recA*$^-$ strain of *Escherichia coli*, and purified as previously described for wild-type KGPDC (*6*).

Protein Purification and Crystallization. KGPDC was expressed and purified as described previously (*6*). The protein was dialyzed against 50 mM HEPES, pH 7.5, 5 mM $MgCl_2$, 100 mM NaCl, concentrated to 15 mg/mL, frozen as small pellets in liquid nitrogen, and stored at −80 °C. Crystals of KGPDC were grown by microbatch by combining 10 μL of protein solution and 10 μL of a solution containing 16% MePEG 5000, 100 mM bis-tris-propane pH 7.0, 5 mM $MgCl_2$, and 25 mM L-xylulose 5-phosphate or 25 mM D-ribulose 5-phosphate as described before (*1*, *15*). All three of the KGPDC mutants crystallized in the space group C2 with two KGPDC molecules in the asymmetric unit. Cell dimensions for each complex after freezing are given in Table 1.

Crystal Freezing and Data Collection. Crystals of all four KGPDC complexes were transferred in two steps for approximately 30 s to a cryoprotecting solution containing 15% MePEG 5000, 100 mM PIPES, pH 7.0, 15% ethylene glycol, 200 mM NaCl, and 50 mM L-threonohydroxamate 4-phosphate or 50 mM D-ribulose 5-phosphate. The crystals were flash frozen in a cold nitrogen stream at −160 °C prior to data collection. Data for wild-type KGPDC, the E112D/T169A KGPDC double mutant, and the E112D/R139V/T169A KGPDC triple mutant with bound D-ribulose 5-phosphate were collected to 2.0, 1.6, and 1.8 Å resolution, respectively. Data for the E112D/R139V/T169A triple mutant with bound L-xylulose 5-phosphate were collected to 1.7 Å resolution. All diffraction data were collected at beamline 19ID of the Structural Biology Center at the Advanced Photon Source, Argonne National Laboratory, Argonne, IL (APS), utilizing a single 180° scan with 1° oscillations for a duration of 5 s per frame. The data were integrated and scaled using HKL2000 (*16*). Data collection statistics are given in Table 1

Structure Determination and Refinement. The structure of each KGPDC mutant was solved by molecular replacement with the program Molrep using the previously determined structure of KGPDC·L-gulonate 6-phosphate as a search model (*1*, *17*, *18*). Each model was improved by refinement with the program Refmac (*17*, *19*, *20*). Solvent atoms were added to each model using the program ARP/wARP (*21*). Final values for the *R*-factor and *R*-free for each structure are listed in Table 2. Analysis with the program PROCHECK indicated that 93.9% of residues were found in the most favorable regions and 6.1% in the additionally allowed regions of a Ramachandran plot for the KGPDC·D-ribulose 5-phosphate structure (*22*). For the E112D/T169A·D-ribulose 5-phosphate structure, 93.5% of the residues fall in the most favorable regions with the remaining 6.3% and 0.3% falling in the additionally allowed and generously allowed regions. For the E112D/R139V/T169A·D-ribulose 5-phosphate structure, 94.8% of the residues fall in the most favorable regions with the remaining 5.2% falling in the additionally allowed regions. For the E112D/R139V/T169A·L-xylulose 5-phosphate structure, 94.8% of the residues fall in the most

Table 2: Refinement Statistics

	WT·D-R5P	E112D/T169V·D-R5P	E112D/R139V/T169A·D-R5P	E112D/R139V/T169A·L-X5P
resolution limits (Å)	91−1.66	91−1.58	91−1.81	91−1.80
R-factor (%)	16.2	15.8	14.3	16.9
R-free (%)	19.4	19.2	17.8	20.9
no. of reflns (working set)	51641	58962	40307	40620
no. of reflns (test set)	2762	3142	2143	2157
no. of protein atoms	3265	3264	3264	3256
no. of solvent atoms	455	507	511	408
av *B* factor (Å^2)	20.6	18.7	14.1	20.3
RMS bond lengths (Å)	0.018	0.018	0.017	0.015
RMS bond angles (deg)	1.65	1.66	1.54	1.47

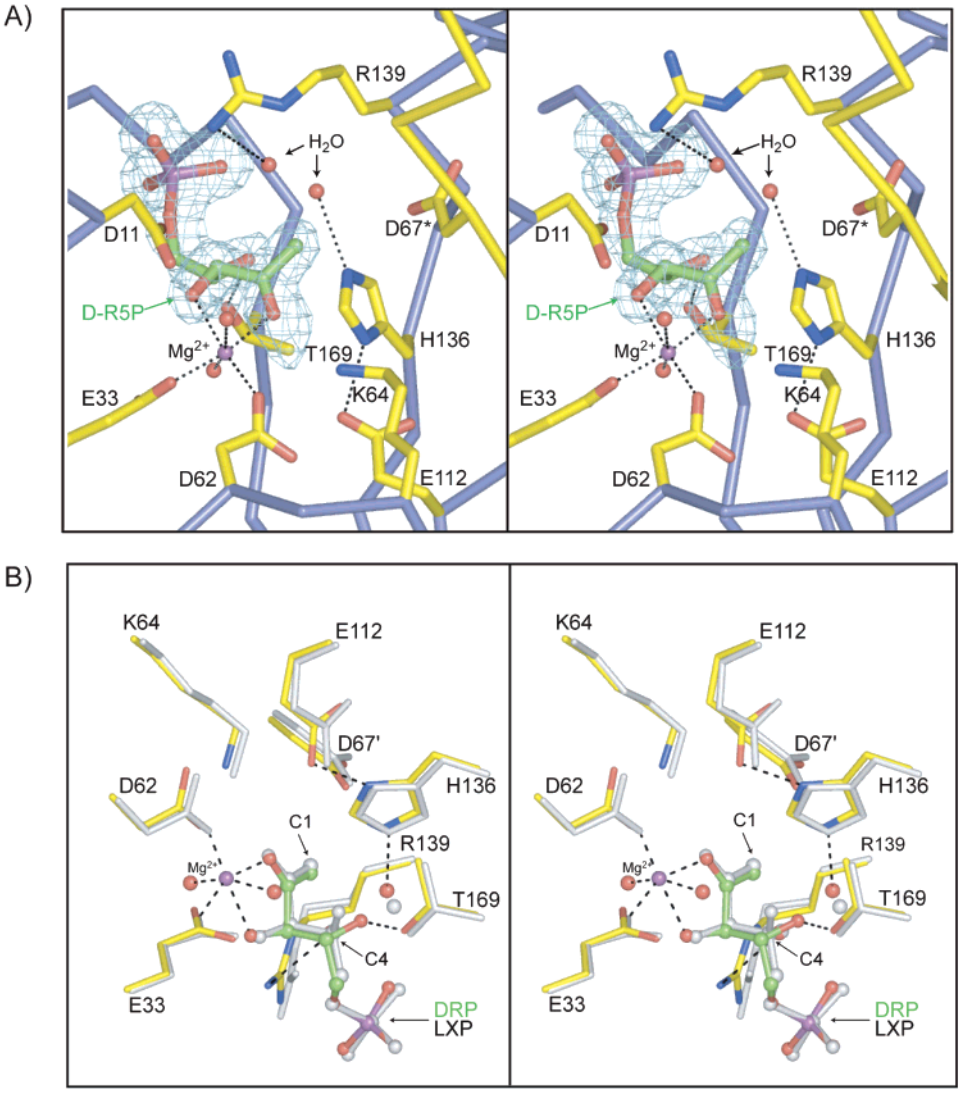

FIGURE 2: (A) Stereoview of the active site of KGPDC with D-ribulose 5-phosphate bound. Electron density, calculated from an omit map, for D-ribulose 5-phosphate is contoured at 3σ. (B) Overlay of the active site of the KGPDC·D-ribulose 5-phosphate structure (yellow) with the KGPDC·L-xylulose 5-phosphate structure (gray). Interactions between both substrates' active site residues and the catalytic Mg^{2+} ion are nearly identical.

favorable regions with the remaining 5.2% falling in the additionally allowed regions. Sample electron density for the KGPDC·D-ribulose 5-phosphate structure is shown in Figure 2A.

RESULTS AND DISCUSSION

Structure of KGPDC with Bound D-Ribulose 5-Phosphate. To understand better how KGPDC catalyzes the promiscuous aldol condensation of D-ribulose 5-phosphate and formaldehyde, the crystal structure of wild-type KGPDC was determined with D-ribulose 5-phosphate bound in the active site. As in previously determined structures of KGPDC, the enzyme assembles as a dimer of $(\beta/\alpha)_8$-barrels that are related by a 2-fold rotational axis that results in the formation of two active sites at the dimer interface (*13*). The position of D-ribulose 5-phosphate in the active site is similar to that

observed for the L-xylulose 5-phosphate product of the KGPDC reaction. Like the structure of KGPDC with L-xylulose 5-phosphate, O1 of the D-ribulose 5-phosphate substrate was not visible in the electron density. As in the other liganded structures of KGPDC, a Mg^{2+} ion was coordinated to O2 and O3 of D-ribulose 5-phosphate as well as the side chains of Glu 33 and Asp 62. The side chain of His 136, which has been implicated in protonation of the enediolate intermediate in the KGPDC-catalyzed reaction, was located near C1 of the D-ribulose 5-phosphate. From the electron density, the change in configuration at carbon C4 that distinguishes D-ribulose 5-phosphate and L-xylulose 5-phosphate could clearly be seen (Figure 2A). Somewhat surprisingly, as in the structure with L-xylulose 5-phosphate, O4 of D-ribulose 5-phosphate forms a hydrogen bond with the side chain of Thr 169 despite the change in configuration at this carbon (Figure 2B). As a result, D-ribulose 5-phosphate adopts a conformation distinct from that of bound L-xylulose 5-phosphate through subtle conformational changes.

The manner in which D-ribulose 5-phosphate binds in the active site of KGPDC is expected to allow the KGPDC-catalyzed HPS reaction to proceed via a 1,2-*cis*-enediolate intermediate similar to that established for the KGPDC reaction. In the natural KGPDC reaction, electrostatic interactions between the Mg^{2+} ion and the negatively charged O2 of the 1,2-enediolate intermediate stabilize the intermediate (*13*). Identical interactions between O2 of D-ribulose 5-phosphate and the Mg^{2+} ion should serve a similar function in the promiscuous HPS reaction and allow KGPDC to stabilize the enediolate formed from D-ribulose 5-phosphate. In addition, the side chains of Lys 64 and Asp 67, both of which stabilize the enediolate in the natural KGPDC reaction, are found in identical positions in the presence of D-ribulose 5-phosphate and likely serve a similar function in the promiscuous HPS reaction.

In the KGPDC reaction, His 136 has been demonstrated to function as a proton source to transfer a proton, via an intermediary water molecule, to C1 of the 1,2-enediolate intermediate to generate L-xylulose 5-phosphate (*13*). The position of the His 136 side chain is virtually unchanged in the presence of D-ribulose 5-phosphate compared to L-xylulose 5-phosphate, so it is expected to participate as the general base in enolization of D-ribulose 5-phosphate in the HPS reaction. In support of this hypothesis, the H136A mutant of KGPDC is unable to catalyze proton exchange of the C1 proton of either L-xylulose 5-phosphate or D-ribulose 5-phosphate and is also unable to catalyze the HPS reaction (*14*).

A solvent-exposed area located on the opposite face of the C1−C2 bond of the bound D-ribulose 5-phosphate provides sufficient room for formaldehyde to approach the 1,2-enediolate and undergo the aldol condensation. Such a mechanism is consistent with the observed stereochemistry for the KGPDC-catalyzed HPS reaction in which the 1-pro*S* proton of D-ribulose 5-phosphate is abstracted and formaldehyde adds to the *re*-face of C1 of the 1,2-enediolate intermediate.

*Structural Bases for the Enhanced HPS Activity of the E112D/T169A Mutan*t. To better understand why the E112D/T169A mutant of KGPDC catalyzes the promiscuous HPS reaction better than either single mutant, the crystal structure of the mutant was determined with D-ribulose 5-phosphate bound. These two mutations have the effect of making KGPDC more "HPS-like": E112D is expected to generate a His 136-Asp 112 dyad, and T169A is expected to remove the hydrogen bonding interaction with O4 of the bound substrate. These substitutions produce a 60-fold increase in the value of k_{cat} for the promiscuous HPS reaction (*14*). Both substitutions could clearly be discerned in the electron density map. The shorter Asp 112 side chain could be differentiated from the longer glutamate side chain in the structure of wild-type KGPDC, and the T169A substitution was unambiguous (Figure 3A). The electron density for D-ribulose 5-phosphate was clear, and the configurational change at C4 compared to L-xylulose 5-phosphate was obvious.

In the structures of wild-type KGPDC with either L-xylulose 5-phosphate or D-ribulose 5-phosphate bound, the side chain of Thr 169 was observed to form a hydrogen bond with O4 of the substrate. This interaction caused D-ribulose 5-phosphate to shift slightly in the active site compared to the position of L-xylulose 5-phosphate due to the difference in configuration about C4 (Figure 3A). The change of Thr 169 to an alanine allows the conformation of D-ribulose 5-phosphate to relax to a conformation more like that of L-xylulose 5-phosphate, which likely allows the 1,2-enediolate intermediate to be stabilized in a more productive conformation.

The significance of the Glu 112 to aspartate substitution is less clear. Much like Glu 112 in the wild-type enzyme, Asp 112 forms a hydrogen bond with Nδ of His 136 and thereby slightly repositions the imidazole group. His 136 moves 0.4 Å closer to the positions of both Asp 112 and C1 of D-ribulose 5-phosphate. In the KGPDC reaction catalyzed by the wild-type enzyme, His 136 was proposed to transfer a proton to C1 of the enediolate D-ribulose 5-phosphate via an intervening water molecule. In the mutant, the shorter Asp 112 moves His 136 closer to C1 of the D-ribulose 5-phosphate so that it now likely can directly mediate proton abstraction.

That the increase in the promiscuous HPS reaction catalyzed by the E112D/T169A mutant is synergistic rather than additive when compared to the activities of the component mutants requires a functional interaction even though these residues are separated by several angstroms. Presumably both affect formation and stabilization of the 1,2-enediolate intermediate: The T169A mutation likely allows the substrate to bind in a conformation that is more conducive for formation of the intermediate, and E112D substitution positions the general base His 136 for direct proton abstraction rather than via a water molecule (Figure 3A).

Structural Bases for Further Increase in HPS Activity in the E112D/R139V/T169A Mutant. The addition of the R139V to the E112D/T169A mutant further enhances the promiscuous HPS reaction: the triple mutant exhibits a 260-fold increase in the value of k_{cat}/K_m relative to wild-type KGPDC, a 6-fold increase relative to the value for the double mutant (*14*). The triple mutant was crystallized in the presence of D-ribulose 5-phosphate. From the electron density all three substitutions were clear. The electron density for the bound D-ribulose 5-phosphate was clear, and the stereochemical configuration about C4 was unambiguous (Figure 3B). As in the structure of the liganded E112D/T169A mutant, the

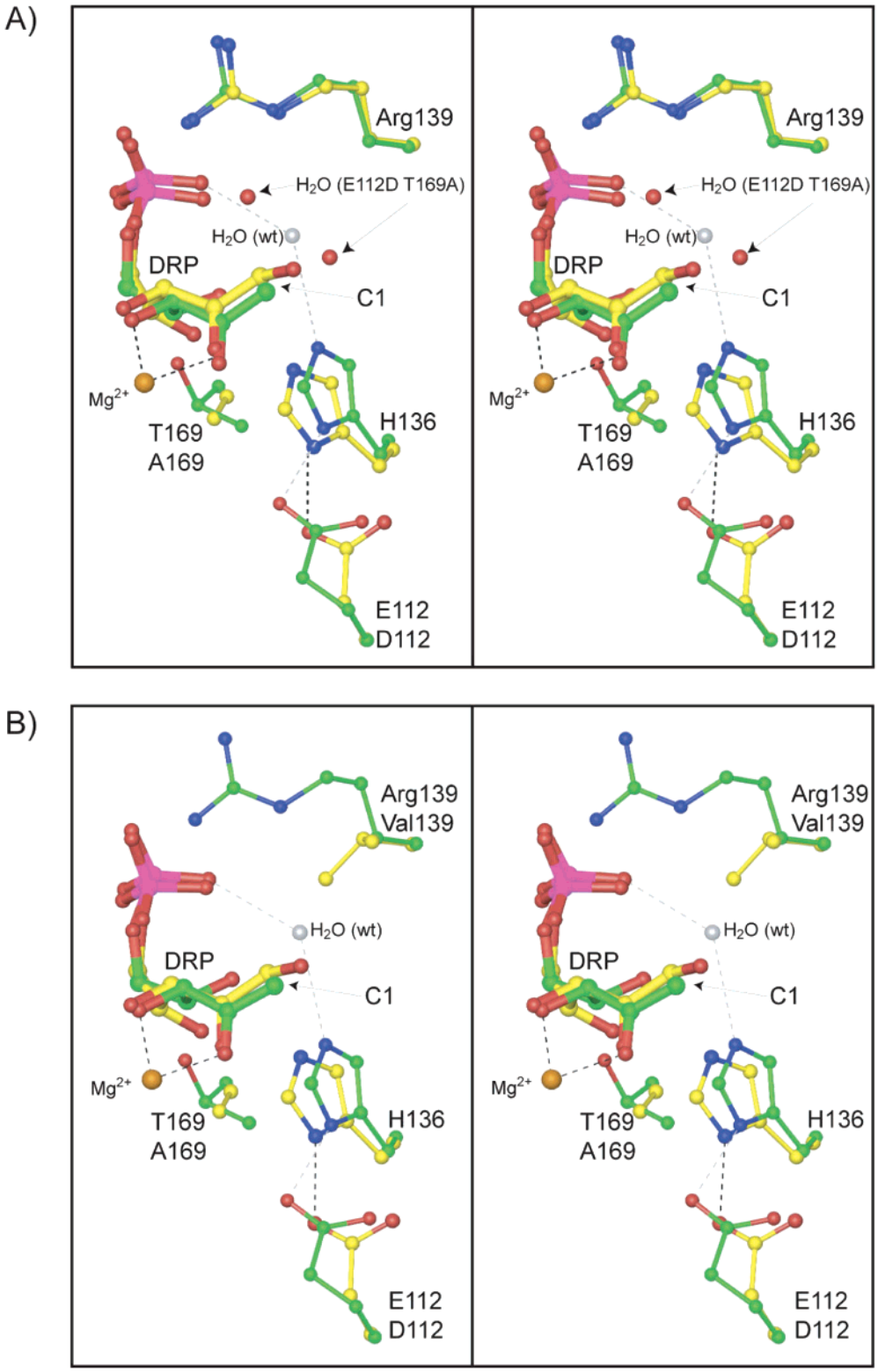

FIGURE 3: (A) Stereoview of the active site of the E112D/T169A double mutant with D-ribulose 5-phosphate bound (yellow) overlaid on top of the structure of wild-type enzyme (green). The glutamate to aspartate substitution causes a shift in the position of the His136 side chain. The threonine to alanine substitution causes a change in the conformation of the substrate. (B) Stereoview of the active site of the E112D/R139V/T169A triple mutant (yellow) overlaid on top of the wild-type enzyme (green). The addition of the arginine to valine mutation results in the absence of ordered water molecules adjacent to C1 of the substrate and may allow greater accessibility for formaldehyde to bind.

shorter Asp 112 pulls His 136 closer to C1 of the bound D-ribulose 5-phosphate.

In this structure, both water molecules that were associated with proton transfer from His 136 and Arg 139 to either face of the 1,2-enediolate are conspicuously absent, while most other ordered water molecules observed in the active site of wild-type KGPDC remain in essentially identical positions. In the natural KGPDC reaction catalyzed by the wild-type protein, Arg 139 has been proposed to transfer a proton via an intervening water molecule to the *re*-face of C1 of the

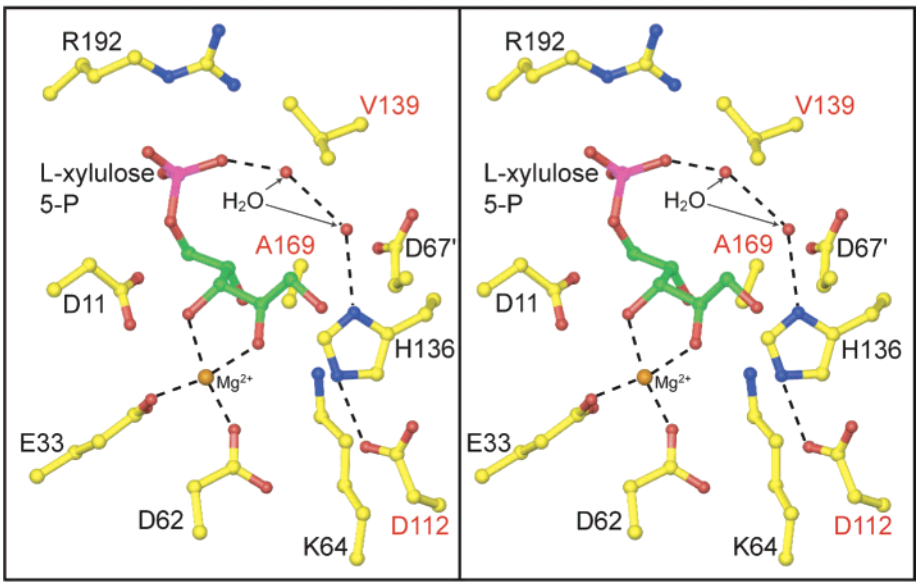

FIGURE 4: Stereoview of the active site of the E112D/R139V/T169A triple mutant with bound L-xylulose 5-phosphate. In the presence of the decarboxylation reaction product, ordered water molecules, associated with the protonation step in the decarboxylation reaction, are observed in the active site, unlike when D-ribulose 5-phosphate is bound.

1,2-enediolate intermediate to generate L-xylulose 5-phosphate. Therefore, the replacement of Arg 139 with Val may improve the access of the electrophilic formaldehyde to the enediolate intermediate, thereby enhancing the efficiency of the promiscuous HPS reaction.

Taken together, the structures of the E112D/T169A and E112D/R139V/T169A mutants suggest that the D-ribulose 5-phosphate substrate for the promiscuous HPS reaction must be correctly positioned for enhanced enolization (E112D and T169A) and subsequent reaction with a proximal formaldehyde (R139V).

Ability of Mutants To Catalyze the Natural KGPDC Reaction. Although the substitutions for Glu 112, Arg 139, and Thr 169 can significantly enhance the promiscuous HPS reaction, their effects on the natural KGPDC reaction are more modest. In order to understand this effect, the structure of the E112D/R139V/T169A mutant was determined in the presence of the L-xylulose 5-phosphate product of the natural KGPDC reaction. Surprisingly, significant changes in active site geometry were observed compared to the complex of the same mutant liganded with the 4-epimeric D-ribulose 5-phosphate. The region surrounding Val 139 was clearly defined for the triple mutant in the presence of D-ribulose 5-phosphate, but the region from Arg 137 to Gly 150 was not well ordered in the presence of L-xylulose 5-phosphate; indeed, Val 139 was not visible. Perhaps more surprising is the effect of the configuration of the bound ligand on the ordered, general acidic water molecules observed in the complex of wild-type KGPDC with L-xylulose 5-phosphate. These are absent in the complex of the triple mutant with D-ribulose 5-phosphate but are present in the complex with L-xylulose 5-phosphate (Figure 4). Thus, the configuration of C4 of the bound ligand can trigger a structural change between the presence of the ordered, acidic water molecules required for the KGPDC reaction and their absence to allow unimpeded access of formaldehyde to the enediolate intermediate in the HPS reaction.

Implications for Enzyme Evolution. The promiscuity of wild-type KGPDC may provide a snapshot of a step in a pathway for divergent evolution of function: the same active site can catalyze either the natural decarboxylation of 3-keto-L-gulonate 6-phosphate or the promiscuous aldol condensation between D-ribulose 5-phosphate and formaldehyde, albeit with different efficiencies. Both reactions involve the Mg^{2+}-dependent stabilization of a 1,2-enediolate intermediate, although the mechanisms by which the intermediates are formed and are partitioned to products are distinct. Our discovery that a limited number of substitutions can dramatically enhance the efficiency of the promiscuous reaction emphasizes that the active site of KGPDC is poised to evolve. Changes in (1) the position the general base His 136 induced by the E112D substitution, (2) the conformation of both the bound substrate and the resulting enediolate intermediate induced by the T169A substitution, and (3) access of formaldehyde to the enediolate intermediate induced by the R139V substitution together enhance the efficiency of the promiscuous aldol condensation. Presumably, selective pressure could have allowed Nature to identify remote substitutions that would further enhance the efficiency to the level observed for wild-type HPS, if KGPDC were the progenitor of HPS.

CONCLUSIONS

In the absence of a structure for a wild-type HPS, we have been able to enhance the promiscuity of KGPDC for catalysis of the HPS reaction. Our sequence-based choice of substitutions was based on mimicking the observed differences in conserved residues that are associated uniquely with the natural KGPDC- and HPS-catalyzed reactions. From the outset, it was difficult to predict the effects of the substitutions on the structure of the active site and how these would alter the efficiency of the HPS reaction, though, of course, the structure of the native enzyme was a great help in guiding the choice of mutations. From the structural information presented in this manuscript, however, it must be recognized that subtle structural changes can have profound but readily rationalized effects on catalysis. The success of this endeavor also emphasizes that evolution of new functions in proteins

possessing the $(\beta/\alpha)_8$-barrel fold can be readily achieved by altering the identities of the residues positioned at the ends of the component β-strands that form the active site. Substitutions in these structurally independent positions can produce synergistic changes in catalytic activity, thereby highlighting the utility of this fold in the divergent evolution of new functions.

REFERENCES

1. Wise, E., Yew, W. S., Babbitt, P. C., Gerlt, J. A., and Rayment, I. (2002) Homologous (beta/alpha)8-barrel enzymes that catalyze unrelated reactions: orotidine 5′-monophosphate decarboxylase and 3-keto-L-gulonate 6-phosphate decarboxylase, *Biochemistry 41*, 3861−9.
2. Feng, W. Y., Austin, T. J., Chew, F., Gronert, S., and Wu, W. (2000) The mechanism of orotidine 5′-monophosphate decarboxylase: catalysis by destabilization of the substrate, *Biochemistry 39*, 1778−83.
3. Cui, W., DeWitt, J. G., Miller, S. M., and Wu, W. (1999) No metal cofactor in orotidine 5′-monophosphate decarboxylase, *Biochem. Biophys. Res. Commun. 259*, 133−5.
4. Miller, B. G., and Wolfenden, R. (2002) Catalytic proficiency: the unusual case of OMP decarboxylase, *Annu. Rev. Biochem. 71*, 847−85.
5. Appleby, T. C., Kinsland, C., Begley, T. P., and Ealick, S. E. (2000) The crystal structure and mechanism of orotidine 5′-monophosphate decarboxylase, *Proc. Natl. Acad. Sci. U.S.A. 97*, 2005−10.
6. Yew, W. S., and Gerlt, J. A. (2002) Utilization of L-ascorbate by Escherichia coli K-12: assignments of functions to products of the yjf-sga and yia-sgb operons, *J. Bacteriol. 184*, 302−6.
7. Ferenci, T., Strom, T., and Quayle, J. R. (1974) Purification and properties of 3-hexulose phosphate synthase and phospho-3-hexuloisomerase from Methylococcus capsulatus, *Biochem. J. 144*, 477−86.
8. Sahm, H., Schutte, H., and Kula, M. R. (1982) 3-Hexulose-phosphate synthase from Methylomonas M15, *Methods Enzymol. 90*, 319−23.
9. Miller, B. G., Snider, M. J., Wolfenden, R., and Short, S. A. (2001) Dissecting a charged network at the active site of orotidine-5′-phosphate decarboxylase, *J. Biol. Chem. 276*, 15174−6.
10. Miller, B. G., Butterfoss, G. L., Short, S. A., and Wolfenden, R. (2001) Role of enzyme-ribofuranosyl contacts in the ground state and transition state for orotidine 5′-phosphate decarboxylase: a role for substrate destabilization?, *Biochemistry 40*, 6227−32.
11. Wise, E. L., Yew, W. S., Gerlt, J. A., and Rayment, I. (2003) Structural evidence for a 1,2-enediolate intermediate in the reaction catalyzed by 3-keto-L-gulonate 6-phosphate decarboxylase, a member of the orotidine 5′-monophosphate decarboxylase suprafamily, *Biochemistry 42*, 12133−42.
12. Yew, W. S., Wise, E. L., Rayment, I., and Gerlt, J. A. (2004) Evolution of enzymatic activities in the orotidine 5′-monophosphate decarboxylase suprafamily: mechanistic evidence for a proton relay system in the active site of 3-keto-L-gulonate 6-phosphate decarboxylase, *Biochemistry 43*, 6427−37.
13. Wise, E. L., Yew, W. S., Gerlt, J. A., and Rayment, I. (2004) Evolution of enzymatic activities in the orotidine 5′-monophosphate decarboxylase suprafamily: crystallographic evidence for a proton relay system in the active site of 3-keto-L-gulonate 6-phosphate decarboxylase, *Biochemistry 43*, 6438−46.
14. Yew, W. S., Akana, J., Wise, E. L., Rayment, I., and Gerlt, J. A. (2004) Evolution of Enzymatic Activities in the Orotidine 5′-Monophosphate Decarboxylase Suprafamily: Enhancing the Promiscuous D-Ararbino-Hex3-ulose 6-Phosphate Synthase Reaction Catalyzed by 3-Keto-L-Gulonate 6-Phosphate Decarboxylase, *Biochemistry*, submitted.
15. Rayment, I. (2002) Small-scale batch crystallization of proteins revisited. An underutilized way to grow large protein crystals, *Structure (Cambridge) 10*, 147−51.
16. Otwinowski, Z., and Minor, W. (1997) Processing of X-ray diffraction data collected in oscillation mode, *Methods Enzymol. 276*, 307−26.
17. CCP4. (1994) The CCP4 Suite: Programs for protein crystallography, *Acta Crystallogr. D50*, 760−3.
18. Vagin, A., and Teplyakov, A. (2000) An approach to multi-copy search in molecular replacement, *Acta Crystallogr., Sect. D: Biol. Crystallogr. 56*, 1622−4.
19. Murshudov, G. N., Vagin, A. A., and Dodson, E. J. (1997) Refinement of Macromolecular Structures by the Maximum-Likelihood Method, *Acta Crystallogr., Sect. D: Biol. Crystallogr. 53*, 240−55.
20. Roussel, A., and Cambillau, C. (1991) Turbo Frodo, in *Silicon Graphics Geometry Partners Directory*, Silicon Graphics, Mountain View, CA.
21. Perrakis, A., Morris, R., and Lamzin, V. S. (1999) Automated protein model building combined with iterative structure refinement, *Nat. Struct. Biol. 6*, 458−63.
22. Laskowski, R. A., MacArthur, M. W., Moss, D. S., and Thornton, J. M. (1993) PROCHECK: a program to check the stereochemical quality of protein structures, *J. Appl. Crystallogr. 26*, 283−91.

BI0478143